ACS APPLIED MATERIALS & INTERFACES

Research Article

www.acsami.org

Tip-Induced Micropatterning of Silk Fibroin Protein Using In Situ Solution Atomic Force Microscopy

Jian Zhong,*[,†] Mengjia Ma,[‡] Juan Zhou,[†] Daixu Wei,[†] Zhiqiang Yan,[†] and Dannong He[†,‡]

[†]National Engineering Research Center for Nanotechnology, Shanghai 200241, People's Republic of China

[‡]School of Materials Science and Engineering, Shanghai Jiao Tong University, Shanghai 200240, People's Republic of China

Supporting Information

ABSTRACT: Silk fibroin (SF) is a promising candidate for a variety of application in the fields of tissue engineering, drug delivery, and biomedical optics. Recent research has already begun to explore the construction of nano- and micropatterned SF films under ambient environment. The structure and biocompatibility of SF are dependent on SF state (solution or solid) and the method of drying the SF solution to prepare various biomaterials such as films, sponges, and fibers. Therefore, it is important to explore the construction of SF nano- and micropatterns under aqueous solution. This paper reports a novel application of atomic force microscopy (AFM) under liquid for direct deposition of the relatively hydrophobic protein SF onto hydrophilic mica. We demonstrate that the AFM tip, in either the contact or the tapping mode, can fabricate SF micropatterns on mica with controlled surface topography. We show that the deposition process requires a mechanical force-induced SF sol–gel transition followed by a transfer to the mica surface at the tip–surface contact, and the efficiency of this process depends on not only AFM operation mode but also the SF bulk concentration, the SF amount on mica, and the AFM tip spring constant.

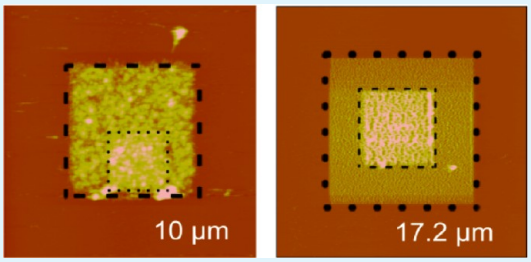

KEYWORDS: *contact mode, in situ solution atomic force microscopy, silk fibroin, sol–gel transition, tapping mode, tip-induced micropatterning*

Stable, precisely controlled, and reproducible micro- and nanopatterning of biomolecules on surfaces has attracted increasing attention in recent years owing to its potential applications in medicine and biotechnology, such as the preparation of biochips and biosensors, drug discovery, and fundamental studies of biological processes.[1,2]

Several types of techniques have been developed to fabricate nano-to-microscale biomolecule architectures, including traditional photolithography,[3,4] microcontact/nanocontact printing,[5,6] electron-beam lithography,[7,8] nanoimprint lithography,[9,10] and scanning probe lithography (SPL).[11] Among these techniques, SPL is a popular high-resolution patterning technique that uses a sharp tip to pattern nano-to-microscale features onto a surface.[12−14] Atomic force microscopy (AFM), a type of scanning probe technique, has been successfully applied to image molecules on the surface,[15] image surface characterization,[16,17] manipulate molecules on the surface,[18−21] and mechanically fabricate 3D nanostructures.[22] On the basis of AFM, many kinds of SPL methods have been developed, including dip-pen nanolithography,[23−25] nanoshaving,[26] nanografting,[27] and so on. These AFM-based lithographic methods have been widely used for the patterning of a large variety of substances such as small organic molecules,[28−30] polymers,[31,32] carbon nanotubes,[33] nanoparticles,[34−36] biological molecules (proteins,[11,37,38] peptides,[39−41] and DNA[42,43]), viruses,[44,45] and bacteria.[46] The patterning of substances by AFM lithography mainly utilizes contact mode AFM. Tapping mode AFM has also already been explored to pattern substances onto a substrate.[47,48] Currently the micro- and nanopatterning of biomolecules by AFM lithography were mainly performed in the ambient air with high humidity. However, low humidity might result in denaturation of biomolecules.[49] It is well-known that the molecule structure and bioactivity of biomolecules in liquid can be more easily kept than in an ambient environment with high humidity. It is important to explore the application of AFM lithography under liquid for the biomolecule deposition where biomolecules are always maintained under liquid and the molecule structure and bioactivity can be easily kept. Though AFM lithography has already been used to pattern small molecules such as lipids[50] and thiols[27] under liquid, to our knowledge, no AFM lithography work of patterning biomacromolecules under liquid has been reported until now. In addition, the AFM-based lithography equipment is generally not available to most scientists. It is important to explore the possibility of patterning molecules using a standard AFM, which will be beneficial to the future application of patterns.

Biomacromolecules, such as silk fibroin (SF), are promising candidates for a variety of applications in the fields of tissue engineering, drug delivery, and biomedical optics. SF protein is a type of natural structural protein of silk produced by *Bombyx*

Received: October 9, 2012
Accepted: December 31, 2012
Published: December 31, 2012

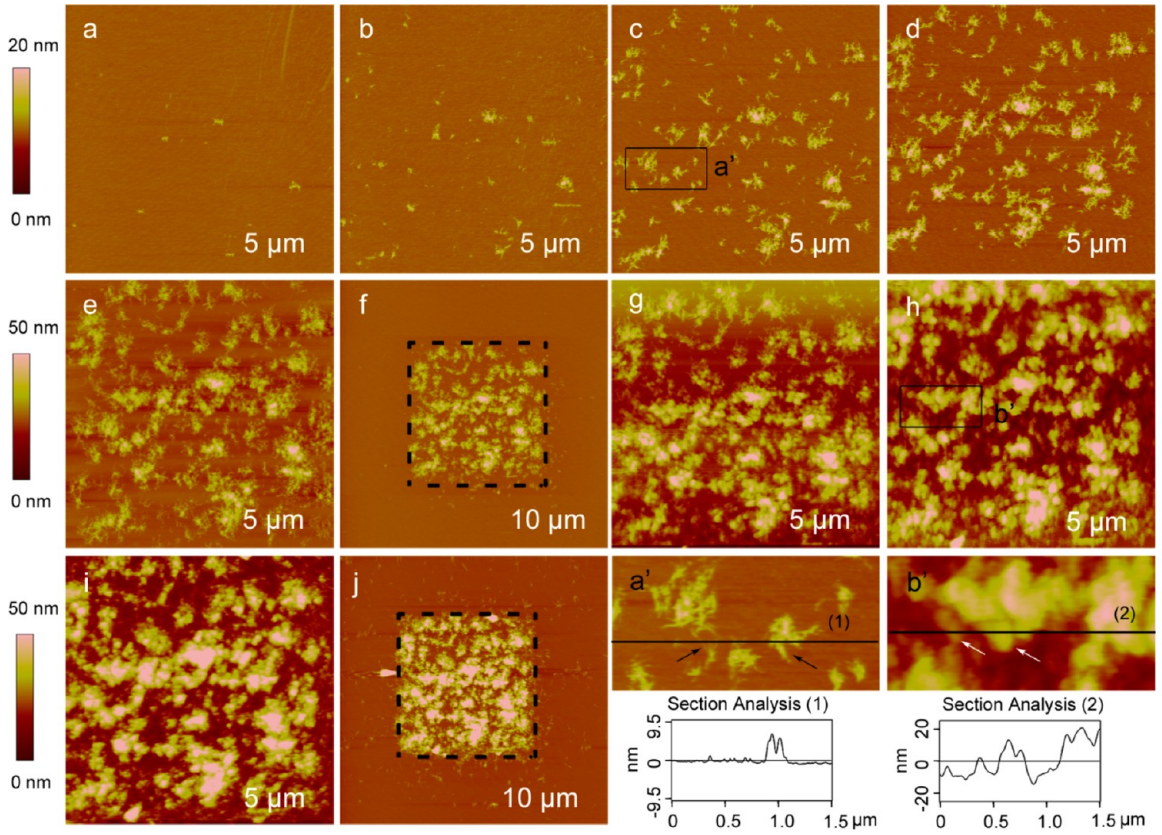

Figure 1. In situ solution tapping mode AFM images of direct SF deposition onto mica using a NP-series silicon nitride tip (0.58 N/m) at a SF bulk concentration of 0.006% (w/w). Height scales for (a–d) and (e–j) are 20 and 50 nm, respectively. (a–e) and (g–i) show the continuous deposition of SF proteins onto the scanning area of mica. (f) and (j) are zoomed out scaning images and show SF proteins only deposited onto the scanning areas (a square of 5 × 5 μm). Times are (a) 8, (b) 25, (c) 50, (d) 67, (e) 111, (f) 120, (g) 129, (h) 146, (i) 180, and (j) 189 min. (a′) and (b′) are zoomed in pictures from the corresponding regions in (c) and (h), respectively. Section Analyses (1) and (2) are along the corresponding black lines in (a′) and (b′), respectively.

mori (mulberry silkworm). SF is a relatively hydrophobic protein consisting of a heavy chain of approximately 390 kDa and a light chain of approximately 25 kDa.[51,52] It has been widely used as textiles for centuries. Due to SF's excellent biocompatibility, high mechanical strength, long-term biodegradability, and low cost, it has been recently explored for nontextile applications such as surgical sutures, wound dressing materials, substrates for cell culture, enzyme immobilization, drug delivery, and scaffolds for bone regeneration and repair.[53−55] Recent research has already begun to explore the construction of nano- and micropatterned SF films under ambient environment for tissue engineering and biomedical optics.[56,57] Nano- and micropatterned SF films were formed by depositing and drying SF solution onto customer-designed templates and then removing the templates. The structure and biocompatibility of SF are dependent on SF state (solution or solid) and the method of drying the SF solution to prepare various biomaterials such as films, sponges, and fibers.[58−61] Therefore, it is important to explore the construction of SF nano- and micropatterns under aqueous solution.

To prepare stable silk patterns under aqueous solution, it is necessary to use hydrophilic substrates such as mica to make sure that the hydrophobic SF molecules do not spontaneously deposit onto the hydrophilic substrates and only AFM tips transfer SF onto the substrates. Herein, we report a novel application for direct micropattern of relatively hydrophobic SF proteins onto mica using in situ solution AFM. Our results confirm that the relatively hydrophobic SF proteins do not spontaneously deposit onto hydrophilic mica under aqueous solution and can be successfully micropatterned onto mica using the AFM tip, in either the tapping or the contact mode. We show that the deposition process requires a mechanical force-induced SF sol–gel transition followed by a transfer to the mica surface at the tip–surface contact, and the efficiency of this process depends on not only the AFM operation mode but also the SF bulk concentration, the SF amount on mica, and the AFM tip spring constant.

RESULTS AND DISCUSSION

Tip-Induced Micropatterning Using in Situ Solution Tapping Mode AFM. Using in situ solution tapping mode AFM with a NP-series silicon nitride tip (the nominal spring constant of the cantilever is 0.58 N/m), a square SF micropattern can be fabricated by scanning the mica surface in ultrapure water. Figure 1 presents a set of in situ time-lapse images of the direct SF deposition on mica at a SF bulk concentration of 0.006% (w/w). The mica was first imaged, and the AFM image showed the mica surface is ultraflat and clean (data not shown). After injection of SF solution, some nanofeatures appeared on the mica at 8 min (Figure 1a). During the AFM tip scanning on the same area (Figure 1a–e and g–i), the deposition amount of the nanofeatures increased over time. An in situ solution tapping mode AFM experiment without the injection of SF proteins showed no nanofeatures

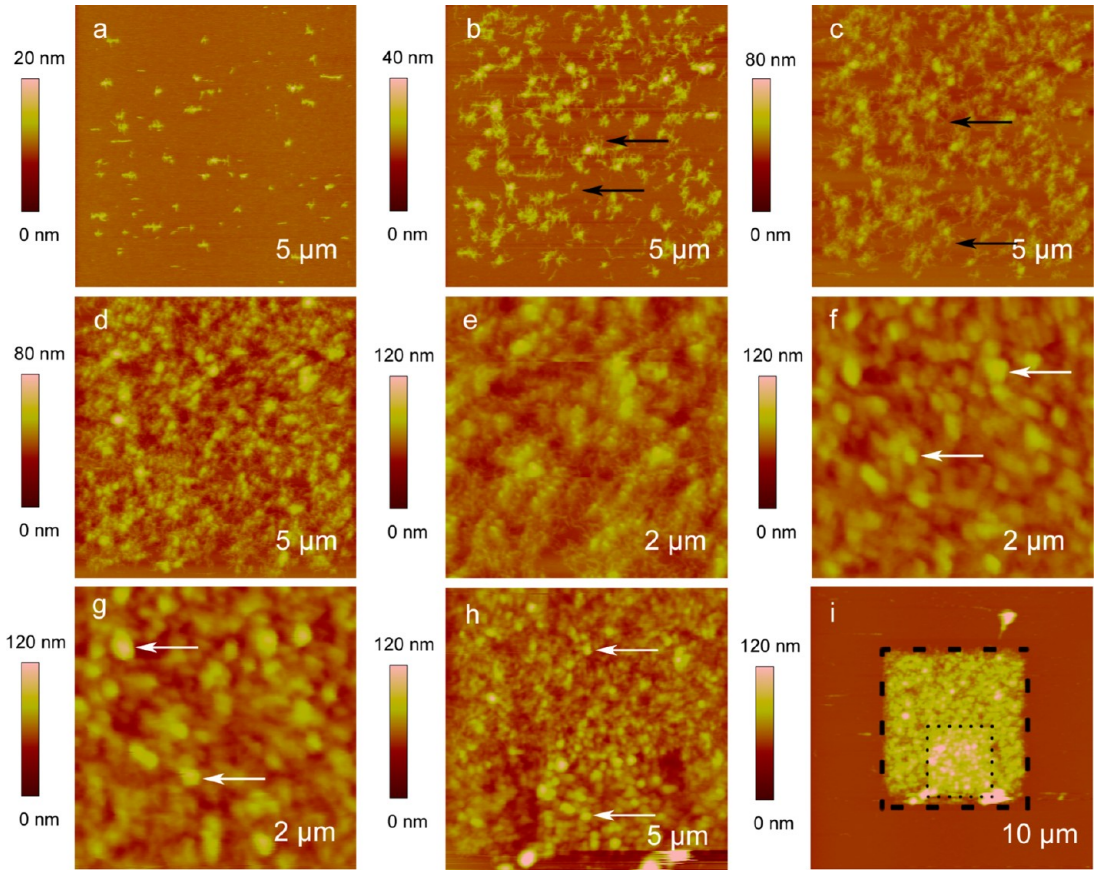

Figure 2. In situ solution tapping mode AFM images of direct SF deposition onto mica using a NP-series silicon nitride tip (0.58 N/m) at a SF bulk concentration of 0.03% (w/w). Height scales are shown on the right of the height images. (a–d) and (e–g) show the continuous deposition of SF proteins onto the scanning area of 5 × 5 μm and 2 × 2 μm, respectively. (h) and (i) are zoomed out images and show SF proteins only deposited onto the scanning areas (squares of 2 × 2 and 5 × 5 μm). Times are (a) 17, (b) 42, (c) 59, (d) 85, (e) 94, (f) 119, (g) 153, (h) 162, and (i) 171 min.

were formed onto the mica even for 3 h (data not shown), which demonstrates the nanofeatures in Figure 1 are SF proteins. The zoomed out scanning images (Figure 1f and j) showed that SF proteins only deposited onto the scanning areas (a square of 5 × 5 μm, indicated by black dashed squares), which demonstrates that relatively hydrophobic SF proteins[51,52] do not spontaneously deposit onto the hydrophilic mica (outside the black dashed squares). Therefore, the main reason for the formation of SF micropatterns is that the AFM tip induces the SF deposition from the solution to the mica in ultrapure water. Figure 1g–j also demonstrates that in situ solution tapping mode AFM can redeposit SF proteins onto a designated region such as the previous deposition area. The heights of SF micropatterns at 120 and 189 min were 13 ± 7 and 21 ± 7 nm, respectively.

Further, the effects of SF bulk concentration on the SF deposition using solution tapping mode AFM with a NP-series 0.58 N/m silicon nitride tip were studied. Figure 2 presents a set of in situ time-lapse images of the direct SF deposition on mica at a SF bulk concentration of 0.03% (w/w). The mica was first imaged, and the AFM image showed the mica surface is ultraflat and clean (data not shown). After injection of SF solution, SF proteins appeared on the mica at 17 min (Figure 2a). During the AFM tip scanning on the same deposition area (Figure 2a–d and e–g), the deposition amount of SF increased over time. The zoomed out scanning image (Figure 2i) further confirms that SF proteins do not spontaneously deposit on mica, and the AFM tip takes the responsibility for the formation of the SF micropattern.

Figure 2i shows the obvious 2 × 2 μm SF micropattern onto the 5 × 5 μm SF micropattern. The heights of 5 × 5 μm and 2 × 2 μm SF micropatterns to mica were 24 ± 7 nm and 43 ± 8 nm, respectively. Therefore, it is possible to redeposit SF proteins onto a SF micropattern to form a complex 3D nanostructure using in situ solution tapping AFM. It took 85 min to deposit a dense 5 × 5 μm SF micropattern with a height of 24 ± 7 nm at a SF bulk concentration of 0.03% (w/w) (Figure 2i). However, it took 120 and 189 min, respectively, to deposit 5 × 5 μm SF deposition features with heights of 13 ± 7 (Figure 1f) and 21 ± 7 nm (Figure 1j), respectively, at a SF bulk concentration of 0.006% (w/w). In addition, the in situ solution tapping mode AFM experiment using a NP-series 0.58 N/m silicon nitride tip at a SF bulk concentration of 0.0015% (w/w) showed no SF proteins were deposited onto the mica even for 3 h (data not shown). Therefore, the SF deposition behavior in solution tapping mode AFM with a NP-series 0.58 N/m silicon nitride tip is dependent on the SF bulk concentration: the critical deposition concentration is 0.006% (w/w), and high SF bulk concentration increases the deposition amount of SF on mica.

Then, to investigate the effect of the AFM tip on the SF deposition, we also tried SNL-series silicon tips (the nominal spring constant of the cantilever is 0.32 N/m) for the tip-induced deposition experiment. Figure 3 presents a set of in situ time-lapse images of the direct SF deposition on mica using

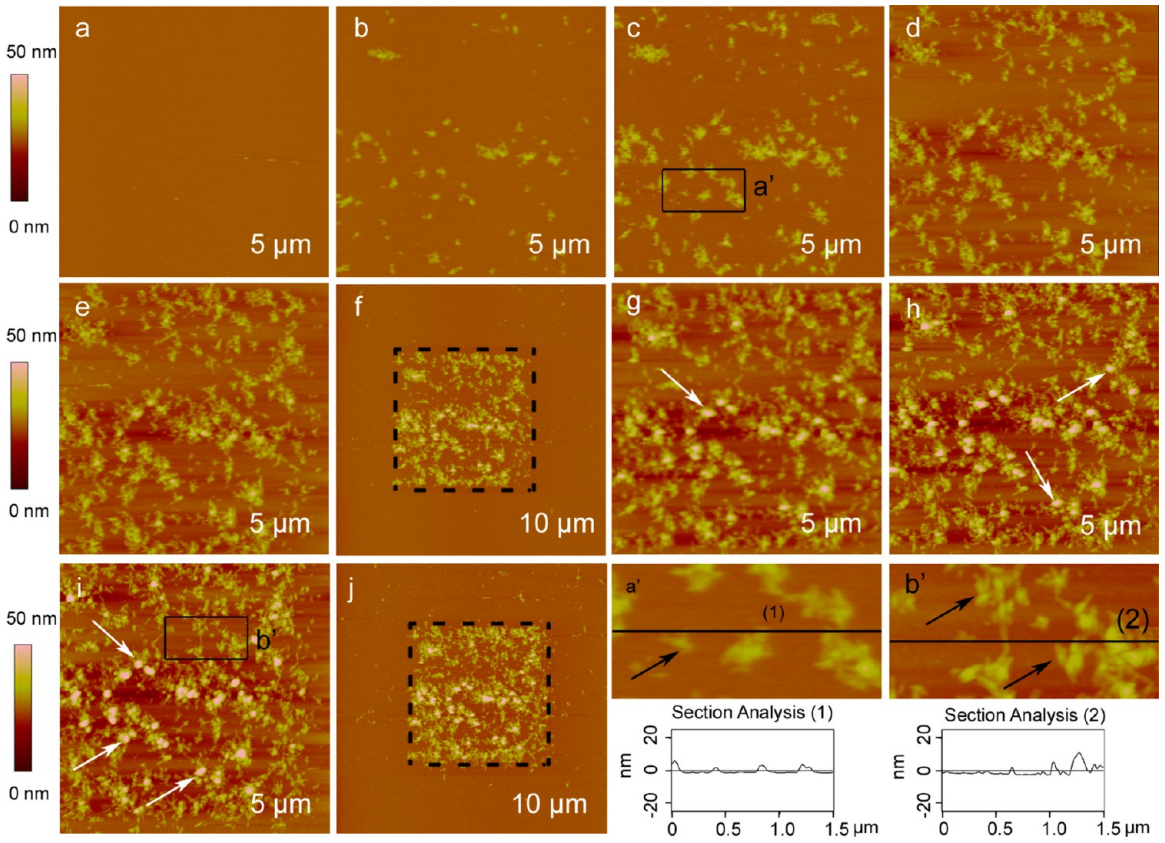

Figure 3. In situ solution tapping mode AFM images of direct SF deposition onto mica using SNL-series silicon tip (0.32 N/m) at a SF bulk concentration of 0.006% (w/w). Height scales are 50 nm. (a–e) and (g–i) show the continuous deposition of SF proteins onto the scanning area of mica. (f) and (j) are zoomed out images and show SF proteins only deposited onto the scanning areas (a square of 5 × 5 μm). Times are (a) 8, (b) 34, (c) 68, (d) 102, (e) 127, (f) 145, (g) 162, (h) 188, (i) 231, and (j) 240 min. (a′) and (b′) are zoomed in pictures from the corresponding regions in (c) and (i), respectively. Section Analyses (1) and (2) are along the corresponding black lines in (k) and (l), respectively.

Table 1. Morphological Sizes of SF Proteins in the Tip-Induced Deposition Experiments Using in Situ Solution Tapping Mode AFM[a]

experiment condition		nanofibrils			nanoparticles	
conc. (w/w)	AFM tip	time (min)	height (nm)	length (nm)	time (min)	diameter[b] (nm)
0.006%	NP 0.58 N/m	8–111	2.8 ± 2.0	116 ± 42	120–189	12 ± 5
0.03%	NP 0.58 N/m	17–85	5.1 ± 1.7	213 ± 62	94–162	39 ± 12
0.006%	SNL 0.32 N/m	8–127	5.4 ± 1.9	127 ± 34	145–240	48 ± 10

[a]The standard deviations were calculated using 30 individual measurements for each parameter. [b]Diameter is the measured height of the SF protein using AFM software.

solution tapping mode AFM with a 0.32 N/m SNL-series silicon tip at a SF bulk concentration of 0.006% (w/w). The mica was first imaged, and the AFM image showed the mica surface is ultraflat and clean (data not shown). After injection of SF solution, SF proteins appeared on the mica at 8 min (Figure 3a). During the AFM tip scanning on the same deposition area (Figure 3a–e and g–i), the deposition amount of SF increased over time. The zoomed out scanning image (Figure 3f and j) further confirms that SF proteins do not spontaneously deposit on mica, and the AFM tip takes the responsibility for the formation of the SF micropattern. Figure 3g–j also demonstrates that in situ solution tapping mode AFM can redeposit SF proteins onto a designated region such as the previous deposition area. The heights of SF deposition features at 145 and 240 min were 8.6 ± 5 and 13 ± 9 nm, respectively. Compared with the NP-series silicon nitride tip (Figure 1f and 1j), the SNL-series silicon tip decreased the SF deposition speed.

Previously, several groups reported the formation of either SF nanofibrils[62,63] or SF nanoparticles[64] at different conditions. Here, SF nanofibrils (indicated by black arrows in Figure 1–3) were formed in the early phase when the local SF content on the mica surface was relatively low, and SF nanoparticles (indicated by white arrows in Figure 1–3) were formed in the later phase when the local SF content on the mica was relatively high. The morphological sizes are summarized in Table 1 and are similar to these previous reports. The tip-induced SF deposition using in situ solution tapping mode AFM demonstrates that the self-assembly of SF proteins is dependent on the SF bulk concentration in solution, SF local content on mica, and AFM tip materials: (1) SF proteins self-assemble into nanofibrils at low local content on mica but form nanoparticles at high local content on mica; (2) high SF bulk concentration

increases the height and length of SF nanofibrils and increases the diameter of SF nanoparticles; (3) compared with the NP-series silicon nitride tip, the SNL-series silicon tip increases the height of SF nanofibrils, decreases the formation of SF nanoparticles, and increases the diameter of SF nanoparticles.

To investigate the role of the AFM tip in the SF deposition on the mica, the AFM tips after the above-mentioned experiments were examined by field emission scanning electron microscopy (FE-SEM) as shown in Figure 4a and 4b.

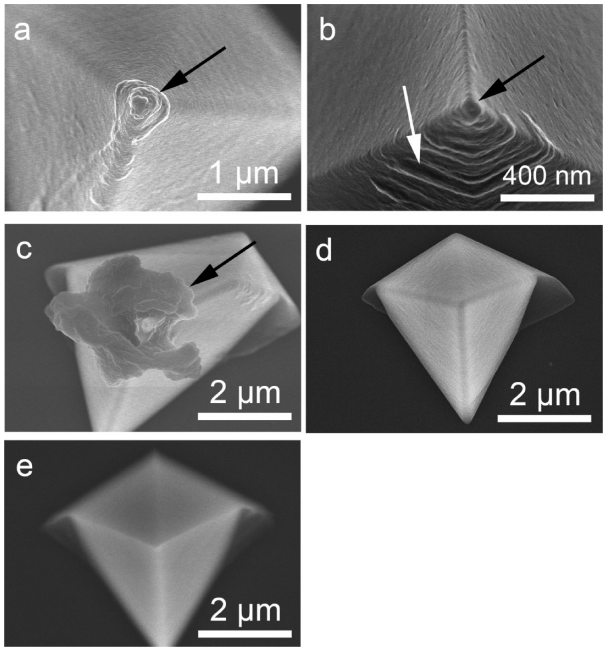

Figure 4. Topographies of AFM tips examined by FE-SEM (a) and (b): the AFM tips located at the end of the NP-series 0.58 N/m and the SNL-series 0.32 N/m cantilever, respectively, after tip-induced SF deposition for 120 min. (c) The AFM tip located at the end of the NP-series 0.12 N/m cantilever after NP-series 0.58 N/m tip-induced SF deposition for 120 min. This NP-series 0.12 N/m tip was oscillated away from the surface during the SF deposition process. (d) and (e): The unused AFM tips located at the end of the NP-series 0.58 N/m cantilever and SNL-series 0.32 N/m cantilever, respectively.

Compared with the clean unused AFM tips (e.g., the unused AFM tips located at the end of the 0.58 N/m NP-series cantilever and 0.32 N/m SNL-series cantilever as shown in Figure 4d and 4e), SF "rings" were shown on the AFM tips located at the end of the NP-series 0.58 N/m cantilever (indicated by a black arrow in Figure 4a) and SNL-series 0.32 N/m cantilever (indicated by a black arrow in Figure 4b). In addition, a SF "flower" (indicated by a black arrow in Figure 4c) was shown on the AFM tip located at the end of the NP-series 0.12 N/m cantilever after the NP-series 0.58 N/m tip-induced SF deposition for 120 min. This NP-series 0.12 N/m tip was oscillated away from the surface during the SF deposition process. Therefore, the amount of SF gels on the AFM tip increased with time. Finally, CD spectra of RSF at different concentrations (Figure 5) present negative adsorption at ~195 nm, a typical characteristic of random coils, which is consistent with previous work of sol–gel transition.[65] Therefore, SF sol–gel transition occurred on AFM tips.

Silk sol–gel transition can be induced by several methods such as electricity,[66] vortexing,[67] shear,[68] pH,[69] temperature,[69] and sonication.[70] Here, the sol–gel transition on the AFM tips

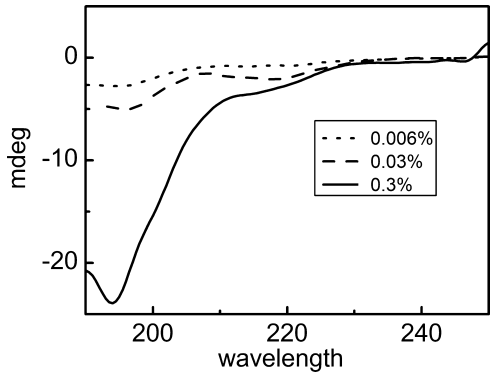

Figure 5. CD spectra of regenerated silk fibroin (RSF) at different concentrations in ultrapure water. All CD spectra present negative adsorption at ~195 nm, a typical characteristic of random coils.

might be induced by electricity or tip oscillations (similar to vortexing). To understand the exact reason, the NP-series 0.58 N/m silicon nitride tip was incubated in a 0.006% (w/w) SF aqueous solution for 140 min, and then the AFM tip was engaged and in situ scanned a 5 × 5 μm mica surface as shown in Figure 6. The results were similar to the experiment where the AFM tip was not incubated in SF solution before in situ scanning (Figure 1), which implies that the tip-induced sol–gel transition results from tip oscillation. Therefore, in the tapping mode AFM, the tip oscillation induces SF sol–gel transition on the AFM tip, and then the tip tapping on the mica surface induces SF deposition.

Compared with the NP-series silicon nitride tip (Figure 4a), there are some wrinkles (indicated by the white arrow in Figure 4b) on the SNL-series silicon tip and less SF proteins (indicated by the black arrow in Figure 4b) on the point of the SNL-series silicon tip, which demonstrate that the SF sol–gel transition mainly occurred on the point of of NP-series 0.58 N/m silicon nitride tip and on the SNL-series 0.32 N/m silicon tip. Considering that the SF sol–gel transition is induced by tip oscillation and the differences of the AFM tips are material (silicon nitride vs silicon) and spring constant (0.58 vs 0.32 N/m), the main reason for the deposition difference might be the difference of the tip spring constant. During the in situ scanning process, the drive frequencies of both the 0.58 N/m NP-series cantilevers and the 0.32 N/m SNL-series cantilevers were selected to 8–9 kHz. Therefore, tip oscillation might not be the main reason for the deposition difference between the two cantilevers. A low spring constant might produce less mechanical force with which the tip is tapping on the surface; therefore, less SF gel forms, and less SF gel is transferred from the AFM tip to the substrate. Hence, the SNL-series 0.32 N/m silicon tip decreases the SF deposition speed (Figure 3 vs Figure 1).

According to the above analyses, we propose that the micropattern of SF proteins on mica in solution tapping mode AFM involves tip-induced deposition. First, the SF sol–gel transition occurs on the AFM tip due to AFM tip oscillation (Figure 9b). Second, the AFM tapping on the mica surface induces that SF gel is transferred to the mica surface (Figure 9c).

Tip-Induced Micropatterning Using in Situ Solution Contact Mode AFM. Solution contact mode AFM was tried for the tip-induced SF deposition experiments. Figure 7 presents a set of in situ time-lapse images of the direct SF deposition on mica using solution contact mode AFM with the

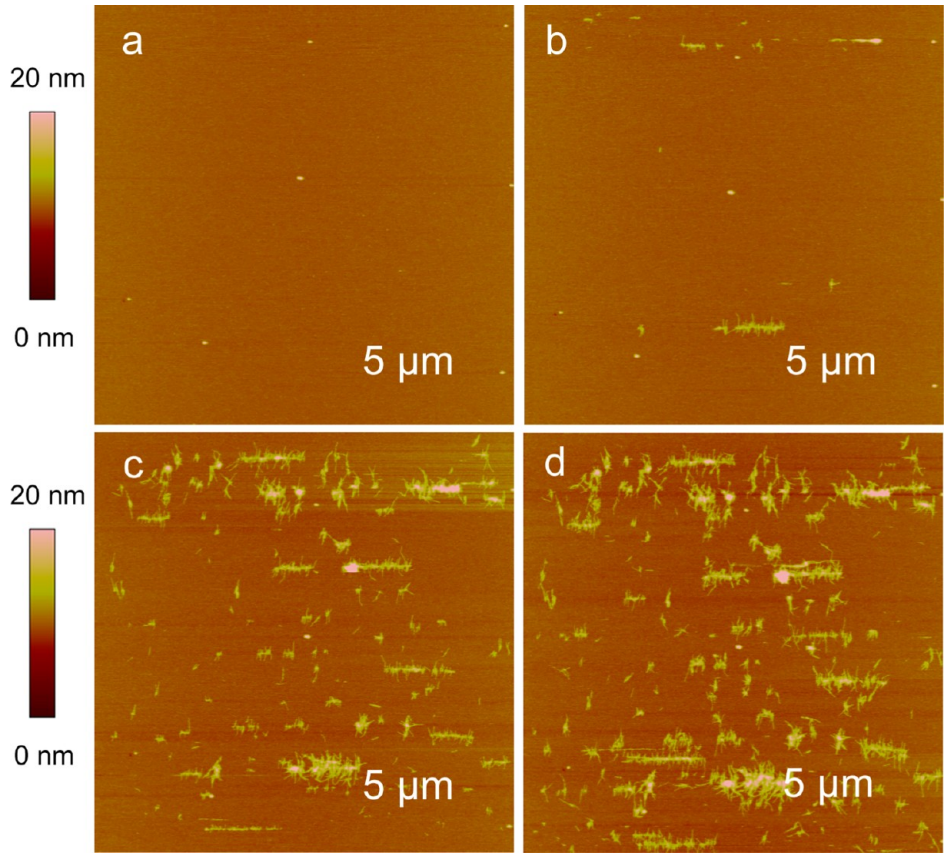

Figure 6. In situ solution tapping mode AFM images of direct SF deposition onto mica using a NP-series silicon nitride tip (0.58 N/m) after 140 min incubation in a 0.006% (w/w) SF aqueous solution. Height scales are 20 nm. Times are (a) 8, (b) 25, (c) 50, and (d) 67.

NP-series 0.58 N/m silicon nitride tip at a SF bulk concentration of 0.03% (w/w). The mica was first imaged, and the AFM image showed that the mica surface is ultraflat and clean (data not shown). After injection of SF solution, SF proteins appeared on the mica at 8 min (Figure 7a). During the AFM tip scanning on the same deposition area (Figure 7a–e and f–i), the deposition amount of SF increased over time. There are mainly nanofibrils on mica during the tip-induced deposition process. The zoomed out scanning images (Figure 7f and j) further revealed SF proteins do not spontaneously deposit on mica, and the AFM tip is the main reason for the formation of the SF micropattern (squares of 5 × 5 and 10 × 10 μm, indicated by black dashed square and black dotted square, respectively). Figure 7f–i also demonstrates that in situ solution contact mode AFM can redeposit SF proteins onto a designated region such as the scanning area which covers a previous one. The height of the SF micropattern at 68 min was 43 ± 17 nm (Figure 7: section analysis (1)). The heights of 5 × 5 μm and 10 × 10 μm SF micropatterns to mica at 128 min were 40 ± 15 nm and 143 ± 44 nm (Figure 7: section analysis (2)), respectively. The height of the 5 × 5 μm SF micropattern at 128 min using contact mode AFM (Figure 7j) was greater than that of the 5 × 5 μm SF micropattern at 171 min using tapping mode AFM (Figure 2i). Moreover, the deposition time of the forth (128 min) was less than that of the latter (171 min). Therefore, the SF deposition in the contact mode AFM is faster than that in the tapping mode AFM. The faster deposition behavior also resulted in that the imaged SF features were a little bit noisy as shown in Figure 7a′. SF nanofibrils were produced in contact mode AFM experiments, while both SF nanofibrils and SF nanoparticles were produced in tapping mode AFM experiments.

Further, using in situ solution contact mode AFM with a NP-series 0.58 N/m silicon nitride tip, as shown in Figure 8, a square SF micropattern (5 × 5 μm) can be generated on mica at a SF bulk concentration of 0.3% (w/w). The height of the SF micropattern was 55 ± 33 nm for a deposition time of 69 min.

We also investigated the effect of low SF bulk concentration in solution on the tip-induced micropatterning. Figures S1 and S2 (Supporting Information) present sets of in situ time-lapse images of the direct SF deposition on mica using solution contact mode AFM with a NP-series 0.58 N/m silicon nitride tip at a SF bulk concentration of 0.006% and 0.0015% (w/w), respectively. Both the AFM experiments showed that the SF deposition features were pushed by a solution contact mode AFM tip. The possible reason is that the tip–surface force in contact mode is enough to push the SF deposition features away. By comparing with the SF deposition amount at the SF bulk concentration of 0.0015% (Figure S2, Supporting Information), 0.006% (Figure S1, Supporting Information), 0.03% (Figure 7), and 0.3% (Figure 8), we can conclude that the SF deposition amount increases with the increase of SF bulk concentration, and the critical micropattern concentration is 0.03% (w/w). Therefore, the sol–gel transition amount increases with the increase of SF bulk concentration.

Considering that the AFM tip is in physical contact with the substrate in contact mode,[71] the permanently shear force on the mica might be the main reason for the sol–gel transition. Therefore, we propose that the micropattern of SF proteins on mica in solution contact mode AFM involves a tip-induced

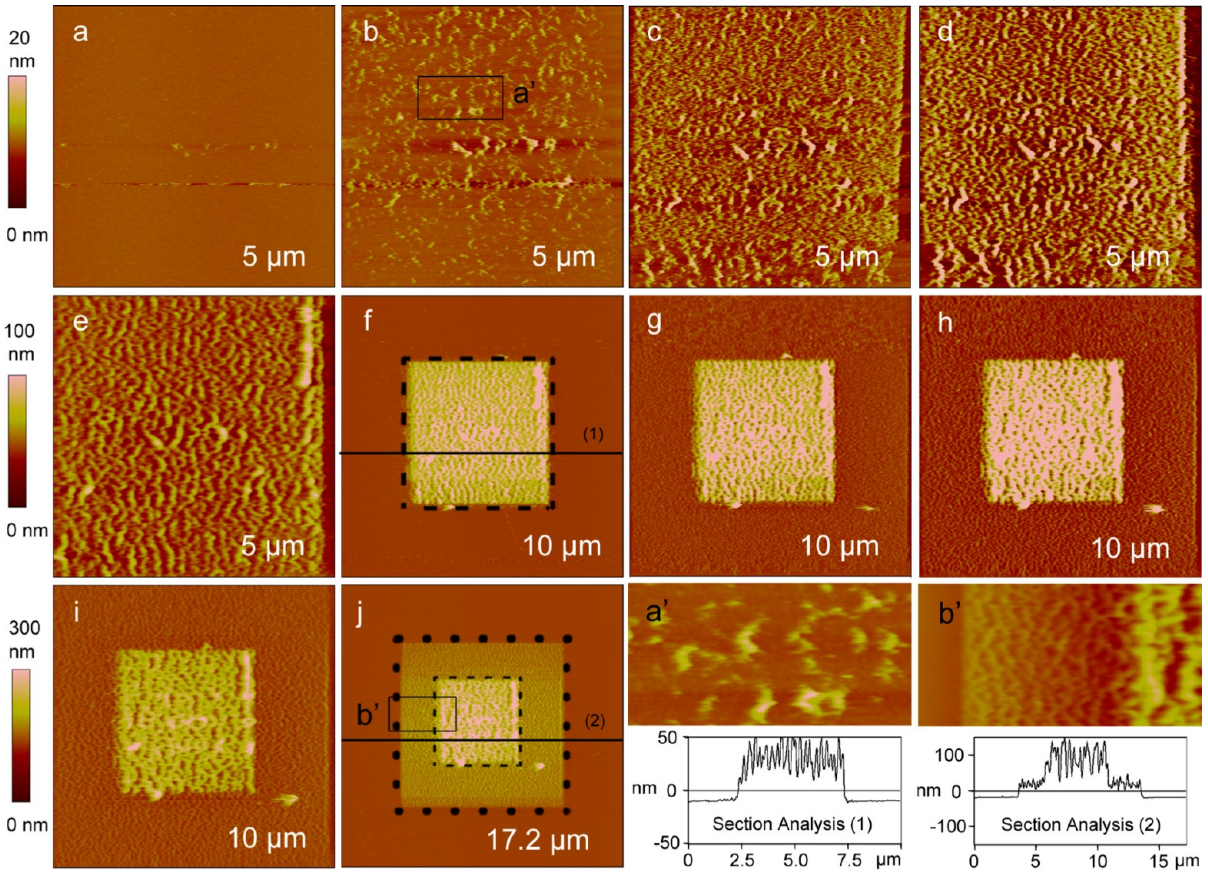

Figure 7. In situ solution contact mode AFM images of direct SF deposition onto mica using a NP-series silicon nitride tip (0.58 N/m) at a SF bulk concentration of 0.03% (w/w). Height scales for (a–d), (e–h), and (i, j) are 20, 100, and 300 nm, respectively. (a–e) and (f–i) show the continuous deposition of SF proteins onto the scanning area of mica. (f) and (j) are zoomed out scaning images and show SF proteins only deposited onto the scanning areas (squares of 5 × 5 and 10 × 10 μm). Times are (a) 8, (b) 17, (c) 25, (d) 34, (e) 59, (f) 68, (g) 85, (h) 102, (i) 119, and (j) 128 min. (a′) and (b′) are zoomed in pictures from the corresponding regions in (b) and (j), respectively. Section Analyses (1) and (2) are along the corresponding black lines in (f) and (j), respectively.

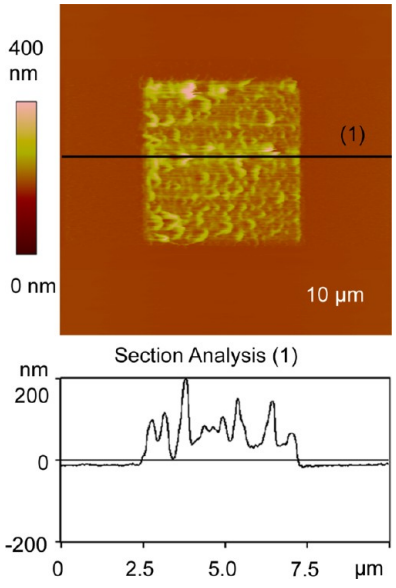

Figure 8. Square SF micropattern of 5 × 5 μm onto mica prepared by in situ solution contact mode AFM with a NP-series silicon nitride tip (0.58 N/m) at a SF concentration of 0.3% (w/w). The deposition time was 69 min. Section Analysis (1) is along the corresponding black line.

deposition process. First, SF sol–gel transition occurs between the tip and surface due to the shear force (Figure 9d). Second, the AFM tip scanning induces that SF gel is transferred to the mica surface (Figure 9e).

One of the grand challenges in nanotechnology is to prepare 3D nanostructures in a controllable, precise, and reproducible fashion.[22] In this work, we showed the SF redeposition processes on the same area (Figure 1g–i and Figure 3g–i), on the smaller area (Figure 2e-g), and on the bigger area (Figure 7f–i). Though these are in a relatively simple layer-on-layer way, considering the development of multiple-pen dip-pen nanolithography techniques,[72,73] we can conclude the feasibility to fabricate SF micropatterns on mica with controllable, reproducible, precise, and complex fashion using in situ solution tapping mode and contact mode AFM. Moreover, our work also demonstrates the possibility of patterning molecules without specialized lithography equipment utilizing a standard AFM, which is available to most university researchers. This work will be beneficial to the future application of SF micropatterns.

CONCLUSIONS

In summary, this paper reported a novel application of in situ solution AFM under liquid for the direct deposition of relatively hydrophobic SF proteins onto hydrophilic mica. We demonstrate that the relatively hydrophobic SF proteins do not

dx.doi.org/10.1021/am302271g | ACS Appl. Mater. Interfaces 2013, 5, 737–746

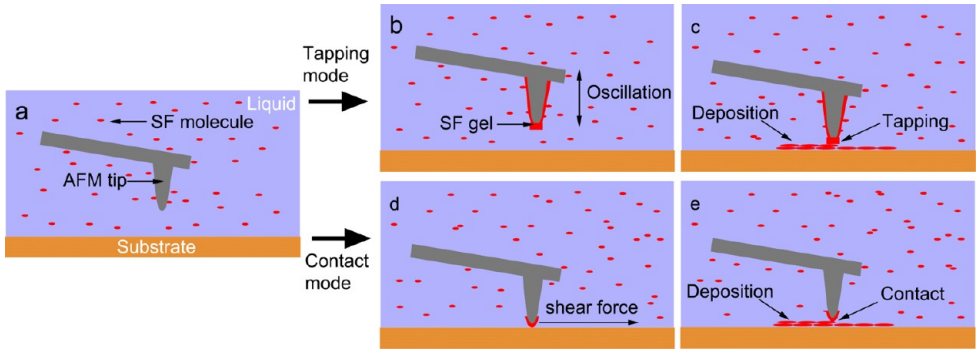

Figure 9. Schematic of direct SF deposition onto mica using in situ solution tapping mode (a–c) and contact mode (a, d, e) AFM. (a): SF proteins were injected into the working liquid. (b): SF sol–gel transition occurred on the AFM tip due to AFM tip oscillation in the tapping mode. (c): The AFM tip tapping on mica induced that the SF gels were slowly deposited to the mica surface. (d): SF sol–gel transition occurred on the AFM tip due to AFM permanently shear force on the mica in the contace mode.(e) The AFM tip scanning on mica induced that the SF gels were slowly deposited to the mica surface.

spontaneously deposit onto the hydrophilic mica. The AFM tip, in either the contact or the tapping mode, can fabricate SF micropatterns on mica with controlled surface topography. We show that the deposition process requires a mechanical force-induced sol–gel transition followed by a transfer to the mica surface at the tip–surface contact, and the efficiency of this process depends on not only the AFM operation mode but also the SF bulk concentration, the SF amount on mica, and the AFM tip spring constant. Solution tapping mode AFM induces less SF deposition than solution contact mode AFM does. In the SF deposition process using solution tapping mode AFM, the critical deposition concentration is 0.006% (w/w). High SF bulk concentration induces larger SF aggregates. SF nanofibrils are formed at low local SF content on the mica surface, and SF nanoparticles are formed at high local SF content on the mica surface. Moreover, compared with the NP-series silicon nitride tip, the SNL-series silicon tip increases the height of SF nanofibrils, decreases the formation of SF nanoparticles, and increases the diameter of SF nanoparticles. In the SF deposition using solution contact mode AFM, the critical micropattern concentration is 0.03% (w/w). SF nanofibrils are mainly formed in the solution contact mode AFM. The sol–gel transition amount and SF deposition amount increase with the increase of SF bulk concentration.

In current mainstream dip-pen nanolithography processes, the transport of biomolecules was performed in ambient air, and low humidity might result in denaturation of biomolecules.[31] Here, our work suggests a possible way to retain the structure and function of biomacromolecules. In addition, this novel application of in situ tapping mode and contact mode AFM under liquid could be combined with multiple-pen dip-pen nanolithography techniques[73] to generate large-scale, parallel, extraordinarily complex nano- and micropatterning of SF proteins, which will be necessary for the application of SF nano- and micropatterns. Moreover, our work also demonstrates the possibility of patterning molecules without specialized lithography equipment utilizing a standard AFM, which is available to most university researchers. Further work will also be necessary to explore the feasibility of the tip-induced deposition to other hydrophobic biomacromolecules. Additional studies must address the effect of the tip-induced deposition process on the biomacromolecule bioactivity. These would increase our understanding of the tip-induced deposition.

MATERIALS AND METHODS

SF proteins were extracted from *Bombyx mori* silkworm cocoons (Huzhou Academy of Agricultural Science, Zhejiang, China) as previously described.[74] Briefly, silkworm cocoons were boiled in 0.5% (w/v) Na_2CO_3 aqueous solution for 30 min and then thoroughly washed with ultrapure water (18 MΩ·cm^{-1}) to remove the glue-like sericin protein. This boiling and washing process was repeated once. The degummed SF was dissolved in a ternary solvent system of $CaCl_2/H_2O/C_2H_5OH$ (1:8:2 in mol ratio) for 40 min at 80 °C. This solution was dialyzed in ultrapure water using dialysis cassettes (MW: 8000–14 000) for 72 h. Finally, the resultant solution was filtered to obtain a pure SF aqueous solution. The final bulk concentration of aqueous SF solution was ~3%, calculated by weighing the remaining solid after drying. The aqueous SF solution was stored at −20 °C immediately after dialysis. The stock solution was thawed prior to the in situ solution tapping mode AFM experiments.

Tip-induced micropatterning by in situ solution tapping mode and contact AFM was performed on a Nanoscope IIIa Multimode AFM (Veeco Instruments, Santa Barbara, CA, USA) with an EV-scanner at room temperature. For our experiments, we used NP-series silicon nitride cantilevers (Veeco Instruments) with a nominal spring constant of 0.58 N/m and SNL-series silicon cantilevers (Veeco Instruments) with a nominal spring constant of 0.32 N/m. In solution tapping mode AFM, the drive frequencies of the cantilevers were selected to 8–9 kHz according to the bandwidth cantilever tune sweep in liquid. For both the tapping mode and contact mode AFM, the tip-induced micropatterning was recorded at a 512 × 512 pixel resolution, and the scan rate was 1.0 Hz. For the tip-induced micropatterning experiments, mica was first imaged in 120 μL of ultrapure water to check the initial state of mica. Then the SF solution was injected into the imaging ultrapure water, and the mica surface was scanned immediately. All the experiments were repeated three times on three independent substrates. All images were analyzed after treatment with "flatten" using Nanoscope III software (version 5.31r1, Veeco Instruments). The height difference was measured using the "section" function, and the surface plot figure was analyzed using the "surface plot" function in the Nanoscope III software.

The topographies of AFM tips were examined by a field emission scanning electron microscope (FE-SEM, Hitachi S-4800) operated at an accelerating voltage of 10 kV.

Circular dichroism spectra were recorded on a Jasco J-815 spectrometer (Tokyo, Japan) at room temperature (about 25 °C). A 1 mm path length cell was employed. Three scans were accumulated and automatically averaged in the wavelength range from 190 to 300 nm with a 1 nm step resolution. Blank ultrapure water measured under the same experimental conditions was subtracted from the data.

■ ASSOCIATED CONTENT

Supporting Information

The effects of low SF bulk concentration in solution on the tip-induced micropatterning. This includes the tip-induced micropatterning processes at two concentrations: 0.006% (w/w) and 0.0015% (w/w). This material is available free of charge via the Internet at http://pubs.acs.org.

■ AUTHOR INFORMATION

Corresponding Author

*E-mail: jianzhongpku@hotmail.com.

Notes

The authors declare no competing financial interest.

■ ACKNOWLEDGMENTS

This research has been supported by research grants from the National Natural Science Foundation of China (51203024), the National High Technology Research and Development Program of China (863 Program 2012AA030309), Shanghai Pujiang Talent Program (12PJ1430300), the Special Fund for Talents in Minhang District of Shanghai (2012), and the Shanghai Municipal Science and Technology Commission (11ZR1425200). We thank Prof. Zhifeng Shao (Shanghai Jiao Tong University) for his helpful discussions and English editing. We also thank the Instrumental Analysis Center of Shanghai Jiao Tong University for the use of Jasco J-815 spectrometer.

■ REFERENCES

(1) Wu, C.-C.; Reinhoudt, D. N.; Otto, C.; Subramaniam, V.; Velders, A. H. *Small* **2011**, *7*, 989−1002.
(2) Falconnet, D.; Csucs, G.; Michelle Grandin, H.; Textor, M. *Biomaterials* **2006**, *27*, 3044−3063.
(3) Schwarz, A.; Rossier, J. S.; Roulet, E.; Mermod, N.; Roberts, M. A.; Girault, H. H. *Langmuir* **1998**, *14*, 5526−5531.
(4) Martin, T. A.; Caliari, S. R.; Williford, P. D.; Harley, B. A.; Bailey, R. C. *Biomaterials* **2011**, *32*, 3949−3957.
(5) Bernard, A.; Renault, J. P.; Michel, B.; Bosshard, H. R.; Delamarche, E. *Adv. Mater.* **2000**, *12*, 1067−1070.
(6) Li, H.-W.; Muir, B. V. O.; Fichet, G.; Huck, W. T. S. *Langmuir* **2003**, *19*, 1963−1965.
(7) Harnett, C. K.; Satyalakshmi, K. M.; Craighead, H. G. *Langmuir* **2000**, *17*, 178−182.
(8) Glezos, N.; Misiakos, K.; Kakabakos, S.; Petrou, P.; Terzoudi, G. *Biosens. Bioelectron.* **2002**, *17*, 279−282.
(9) Truskett, V. N.; Watts, M. P. C. *Trends Biotechnol.* **2006**, *24*, 312−317.
(10) Shi, S.; Lu, N.; Lu, Y.; Wang, Y.; Qi, D.; Xu, H.; Chi, L. *ACS Appl. Mater. Interfaces* **2011**, *3*, 4174−4179.
(11) Lee, K.-B.; Lim, J.-H.; Mirkin, C. A. *J. Am. Chem. Soc.* **2003**, *125*, 5588−5589.
(12) Soh, H. T.; Wilder, G. K.; Quate, C. F. *Scanning probe lithography*; Kluwer Academic Publishers: Norwell, 2001.
(13) Zhou, X.; Boey, F.; Huo, F.; Huang, L.; Zhang, H. *Small* **2011**, *7*, 2273−2289.
(14) Krämer, S.; Fuierer, R. R.; Gorman, C. B. *Chem. Rev. (Washington, DC, U. S.)* **2003**, *103*, 4367−4418.
(15) Czajkowsky, D. M.; Li, L.; Sun, J.; Hu, J.; Shao, Z. *ACS Nano* **2011**, *6*, 190−198.
(16) Pernites, R. B.; Felipe, M. J. L.; Foster, E. L.; Advincula, R. C. *ACS Appl. Mater. Interfaces* **2011**, *3*, 817−827.
(17) Ke, L.; Lai, S. C.; Liu, H.; Peh, C. K. N.; Wang, B.; Teng, J. H. *ACS Appl. Mater. Interfaces* **2012**, *4*, 1247−1253.
(18) Neuman, K. C.; Nagy, A. *Nat. Methods* **2008**, *5*, 491−505.
(19) Kim, M.; Wang, C.-C.; Benedetti, F.; Rabbi, M.; Bennett, V.; Marszalek, P. E. *Adv. Mater.* **2011**, *23*, 5684−5688.
(20) Zhang, F.-C.; Zhang, F.; Su, H.-N.; Li, H.; Zhang, Y.; Hu, J. *ACS Nano* **2010**, *4*, 5791−5796.
(21) Zhang, Y.; Hu, X.; Sun, J.; Shen, Y.; Hu, J.; Xu, X.; Shao, Z. *Microsc. Res. Tech.* **2011**, *74*, 614−626.
(22) Yan, Y.; Hu, Z.; Zhao, X.; Sun, T.; Dong, S.; Li, X. *Small* **2010**, *6*, 724−728.
(23) Piner, R. D.; Zhu, J.; Xu, F.; Hong, S.; Mirkin, C. A. *Science (Washington, DC, U. S.)* **1999**, *283*, 661−663.
(24) Salaita, K.; Wang, Y.; Mirkin, C. A. *Nat. Nanotechnol.* **2007**, *2*, 145−155.
(25) Wang, X.; Wang, X.; Fernandez, R.; Ocola, L.; Yan, M.; La Rosa, A. *ACS Appl. Mater. Interfaces* **2010**, *2*, 2904−2909.
(26) Xu, S.; Liu, G.-y. *Langmuir* **1997**, *13*, 127−129.
(27) Xu, S.; Miller, S.; Laibinis, P. E.; Liu, G.-y. *Langmuir* **1999**, *15*, 7244−7251.
(28) Liu, G.-Y.; Xu, S.; Qian, Y. *Acc. Chem. Res.* **2000**, *33*, 457−466.
(29) Zhang, Y.; Salaita, K.; Lim, J.-H.; Mirkin, C. A. *Nano Lett.* **2002**, *2*, 1389−1392.
(30) Zheng, Z.; Yang, M.; Zhang, B. *J. Phys. Chem. C* **2010**, *114*, 19220−19226.
(31) Noy, A.; Miller, A. E.; Klare, J. E.; Weeks, B. L.; Woods, B. W.; DeYoreo, J. J. *Nano Lett.* **2001**, *2*, 109−112.
(32) Zhou, X.; Liu, X.; Xie, Z.; Zheng, Z. *Nanoscale* **2011**, *3*, 4929−4939.
(33) Zhou, X.; Boey, F.; Zhang, H. *Chem. Soc. Rev.* **2011**, *40*, 5221−5231.
(34) Zheng, J.; Chen, Z.; Liu, Z. *Langmuir* **2000**, *16*, 9673−9676.
(35) Liu, X.; Fu, L.; Hong, S.; Dravid, V. P.; Mirkin, C. A. *Adv. Mater.* **2002**, *14*, 231−234.
(36) Wang, W. M.; Stoltenberg, R. M.; Liu, S.; Bao, Z. *ACS Nano* **2008**, *2*, 2135−2142.
(37) Wu, C.-C.; Reinhoudt, D. N.; Otto, C.; Velders, A. H.; Subramaniam, V. *ACS Nano* **2010**, *4*, 1083−1091.
(38) Wong, L. S.; Karthikeyan, C. V.; Eichelsdoerfer, D. J.; Micklefield, J.; Mirkin, C. A. *Nanoscale* **2012**, *4*, 659−666.
(39) Cho, Y.; Ivanisevic, A. *J. Phys. Chem. B* **2004**, *108*, 15223−15228.
(40) Jiang, H.; Stupp, S. I. *Langmuir* **2005**, *21*, 5242−5246.
(41) Sistiabudi, R.; Ivanisevic, A. *J. Phys. Chem. C* **2007**, *111*, 11676−11681.
(42) Demers, L. M.; Ginger, D. S.; Park, S.-J.; Li, Z.; Chung, S.-W.; Mirkin, C. A. *Science (Washington, DC, U. S.)* **2002**, *296*, 1836−1838.
(43) Onses, M. S.; Pathak, P.; Liu, C.-C.; Cerrina, F.; Nealey, P. F. *ACS Nano* **2011**, *5*, 7899−7909.
(44) Smith, J. C.; Lee, K.-B.; Wang, Q.; Finn, M. G.; Johnson, J. E.; Mrksich, M.; Mirkin, C. A. *Nano Lett.* **2003**, *3*, 883−886.
(45) Cheung, C. L.; Camarero, J. A.; Woods, B. W.; Lin, T.; Johnson, J. E.; De Yoreo, J. J. *J. Am. Chem. Soc.* **2003**, *125*, 6848−6849.
(46) Rozhok, S.; Shen, C. K. F.; Littler, P. L. H.; Fan, Z.; Liu, C.; Mirkin, C. A.; Holz, R. C. *Small* **2005**, *1*, 445−451.
(47) Agarwal, G.; Sowards, L. A.; Naik, R. R.; Stone, M. O. *J. Am. Chem. Soc.* **2003**, *125*, 580−583.
(48) Liang, J.; Scoles, G. *Langmuir* **2007**, *23*, 6142−6147.
(49) Nam, J.-M.; Han, S. W.; Lee, K.-B.; Liu, X.; Ratner, M. A.; Mirkin, C. A. *Angew. Chem., Int. Ed.* **2004**, *116*, 1266−1269.
(50) Lenhert, S.; Mirkin, C. A.; Fuchs, H. *Scanning* **2010**, *32*, 15−23.
(51) Jin, H.-J.; Park, J.; Valluzzi, R.; Cebe, P.; Kaplan, D. L. *Biomacromolecules* **2004**, *5*, 711−717.
(52) Zhou, C.-Z.; Confalonieri, F.; Medina, N.; Zivanovic, Y.; Esnault, C.; Yang, T.; Jacquet, M.; Janin, J.; Duguet, M.; Perasso, R.; Li, Z.-G. *Nucleic Acids Res.* **2000**, *28*, 2413−2419.
(53) Altman, G. H.; Diaz, F.; Jakuba, C.; Calabro, T.; Horan, R. L.; Chen, J.; Lu, H.; Richmond, J.; Kaplan, D. L. *Biomaterials* **2003**, *24*, 401−416.
(54) Vepari, C.; Kaplan, D. L. *Prog. Polym. Sci.* **2007**, *32*, 991−1007.
(55) Porter, D.; Vollrath, F. *Adv. Mater.* **2009**, *21*, 487−492.

(56) Gupta, M. K.; Khokhar, S. K.; Phillips, D. M.; Sowards, L. A.; Drummy, L. F.; Kadakia, M. P.; Naik, R. R. *Langmuir* **2006**, *23*, 1315−1319.
(57) Perry, H.; Gopinath, A.; Kaplan, D. L.; Dal Negro, L.; Omenetto, F. G. *Adv. Mater.* **2008**, *20*, 3070−3072.
(58) Ha, S.-W.; Tonelli, A. E.; Hudson, S. M. *Biomacromolecules* **2005**, *6*, 1722−1731.
(59) Lawrence, B.; Omenetto, F.; Chui, K.; Kaplan, D. *J. Mater. Sci.* **2008**, *43*, 6967−6985.
(60) Kim, U.-J.; Park, J.; Joo Kim, H.; Wada, M.; Kaplan, D. L. *Biomaterials* **2005**, *26*, 2775−2785.
(61) Zuo, B.; Dai, L.; Wu, Z. *J. Mater. Sci.* **2006**, *41*, 3357−3361.
(62) Inoue, S.-I.; Magoshi, J.; Tanaka, T.; Magoshi, Y.; Becker, M. *J. Polym. Sci., Polym. Phys. Ed.* **2000**, *38*, 1436−1439.
(63) Inoue, S.-i.; Tsuda, H.; Tanaka, T.; Kobayashi, M.; Magoshi, Y.; Magoshi, J. *Nano Lett.* **2003**, *3*, 1329−1332.
(64) Zhang, Y.-Q.; Shen, W.-D.; Xiang, R.-L.; Zhuge, L.-J.; Gao, W.-J.; Wang, W.-B. *J. Nanopart. Res.* **2007**, *9*, 885−900.
(65) Matsumoto, A.; Chen, J.; Collette, A. L.; Kim, U.-J.; Altman, G. H.; Cebe, P.; Kaplan, D. L. *J. Phys. Chem. B* **2006**, *110*, 21630−21638.
(66) Leisk, G. G.; Lo, T. J.; Yucel, T.; Lu, Q.; Kaplan, D. L. *Adv. Mater.* **2010**, *22*, 711−715.
(67) Yucel, T.; Cebe, P.; Kaplan, D. L. *Biophys. J.* **2009**, *97*, 2044−2050.
(68) Holland, C.; Urbach, J. S.; Blair, D. L. *Soft Matter* **2012**, *8*, 2590−2594.
(69) Kim, U.-J.; Park, J.; Li, C.; Jin, H.-J.; Valluzzi, R.; Kaplan, D. L. *Biomacromolecules* **2004**, *5*, 786−792.
(70) Wang, X.; Kluge, J. A.; Leisk, G. G.; Kaplan, D. L. *Biomaterials* **2008**, *29*, 1054−1064.
(71) Zhong, J. *Integr. Biol.* **2011**, *3*, 632−644.
(72) Mirkin, C. A. *ACS Nano* **2007**, *1*, 79−83.
(73) Martinez-Otero, A.; Gonzalez-Monje, P.; Maspoch, D.; Hernando, J.; Ruiz-Molina, D. *Chem. Commun. (Cambridge, U. K.)* **2011**, *47*, 6864−6866.
(74) Zhou, J.; Cao, C.; Ma, X. *Int. J. Biol. Macromol.* **2009**, *45*, 504−510.